ARTICLE

Fabrication of Monolayers of Uniform Polymeric Particles by Inkjet Printing of Monodisperse Emulsions Produced by Microfluidics

Yilin Wang, Renhua Deng, Lisong Yang, and Colin D. Bain*

Emulsion solvent evaporation is a well-established method for generating microparticles from solutions of polymers in volatile organic solvents dispersed in an aqueous medium. Previous work has shown that this approach can also be used to deposit particles by inkjet printing where the particles are formed during the drying of a liquid ink on a substrate. The particle size distribution, however, was very broad. Here we demonstrate that inkjet printing of oil-in-water emulsions produced by microfluidics can generate micron-sized particles with a narrow size distribution (coefficient of variation <6%) and that these particles can self-assemble into ordered arrays with hexagonal packing. The conditions under which drops can be printed with a minimum of break up and coalescence of the oil droplets in the emulsion are explored. Factors affecting the size of the particles and the morphology of the deposit are described. This study uses polystyrene in dichloromethane as a model system, but the approach can be generalized to the production of structured and functional particles.

Introduction

Emulsion solvent evaporation is a well-established method for producing microparticles.[1-4] In this approach, polymers and other non-volatile components are dissolved in the discrete phase of an oil-in-water (o/w) emulsion. The non-polar solvent is chosen to be more volatile than the continuous aqueous phase so that the droplets evaporate before the continuous phase to produce discrete particles. Depending on the solutes employed and their phase behaviour, a wide variety of different morphologies can result.

In a previous paper,[5] we have shown that emulsion solvent evaporation can be coupled with inkjet printing to fabricate microparticles of polymers on a surface. The emulsion 'ink' is in the liquid phase and the particles are only generated during the drying process. This approach avoids problems of jetting of inks with micron-sized particles, including blocking of nozzles and variability in the direction of jetting. It also avoids formulation stability issues, such as aggregation and settling of particles. Our previous work used emulsions produced in a homogenizer, which generated a wide range of oil droplet sizes and hence a wide range of particle sizes from sub-micron up to a few microns. The purpose of this paper is to show that the same approach can be used with monodisperse emulsions produced in a microfluidic chip and that these emulsions can be printed with only a small amount of degradation in the size distribution of the oil droplets, thus yielding particles with a narrow distribution of sizes. Coupling of the microfluidic chip to the inkjet nozzle can reduce the time between generation and printing of the emulsion and thus minimise stability issues with the emulsion, such as Ostwald ripening or coalescence.

Our model system comprises polystyrene (PS) dissolved in dichloromethane (DCM) as the oil phase and aqueous solutions of sodium dodecylsulphate (SDS) as the continuous phase. The SDS stabilises the emulsion before printing. Inkjet printing has previously been used to fabricate patterns of colloidal particles via evaporation-induced self-assembly (EISA) of particulate inks drying on a substrate.[6-12] If the particles size is right (hundreds of nm), these patterns can exhibit structural colour, so-called colloidal photonic crystals, which can be used for applications in sensors and displays.[13-18] We can therefore compare the patterns formed by emulsion solvent evaporation of liquids with those from the printing of particulate inks.

Evaporation of a bulk dispersion of colloidal particles on a substrate can generate a 2D film of colloidal crystals.[19-21] It is challenge to design desired patterns unless templates are used.[6, 22] Evaporation of drops of a colloidal dispersion can form spheres/dots of colloidal crystals.[4, 23-26] The drops can be deposited onto substrates to form desired patterns (arrays of dots, lines and large-scale patterns) via inkjet printing.[27-30] Compared to templated assembly, inkjet printing offers the advantages of digital control over patterns, uses less material, allows precise positioning of deposits, is applicable to

a. *Department of Chemistry, Durham University, Stockton Road, Durham DH1 3LE, U.K.*

flexible substrates and is easier to scale-up.

In this paper, we first show that o/w emulsions containing PS/DCM droplets produced in a flow-focussing junction evaporate in a cast film and form monodisperse particles that self-assemble into an ordered hexagonal array. We then show that these same emulsions can be printed successfully to produce dry deposits with a narrow particle size distribution. We discuss how the physics of drying influences this process. The conditions are optimised to minimise the amount of break up and coalescence of droplets during the jetting process and hence to produce particles with a narrow size distribution. Variation in the droplet size and polymer concentration can be used to control the final particle size. We explore the conditions necessary to obtain dense monolayer deposits of both small (~1 μm diameter) and larger (2−3 μm diameter) particles. Finally, we discuss the prospects for manufacturing more complex functional particles by inkjet printing of emulsions and the limitations of the approach.

EXPERIMENTAL SECTION

Materials. Polystyrene (PS, M_W = 35 kg mol^{-1}), sodium dodecyl sulfate (SDS, > 99%), chloro(dimethyl)octylsilane (CDMOS, 97%) and hexamethyldisilazane (HMDS, 98%) were obtained from Sigma-Aldrich; dichloromethane (DCM, >99%) was obtained from Fisher Scientific. All chemicals were used as received.

Preparation of o/w emulsion by microfluidics. Polystyrene was dissolved in DCM to prepare polystyrene solutions with concentrations of 0.5 − 5.0 wt%. SDS was dissolved in deionized water to produce aqueous solutions with concentrations of 0.05 − 1.0 wt %. The solutions were filtered through a 0.2-μm PTFE filter and loaded into two gas-tight borosilicate syringes with PTFE-tipped plungers and luer-lock connectors (1 mL, KR Analyticals). The oil phase and aqueous phase were injected into a microfluidic chip (small quartz droplet chip, 5-μm etch depth and 500-μm channel width, Dolomite) with a flow-focusing junction (5-μm etch depth and 8-μm junction width) via two syringe pumps (AL1000, World Precision Instruments), FEP tubing (1/16" o.d. × 0.25 mm i.d., Dolomite) and connectors (Top Interface 4-way, Linear Connector 4-way, Dolomite). The oil phase was injected into the central channel of the microfluidic chip, and the water phase was divided into two flows via a Y-connector (Y Assembly PEEK, IDEX) before entry into the two side channels of the microfluidic chip. The flow rate of the aqueous phase remained constant at 2 μL /min and the flow rate of the oil phase was varied from 0.2 − 1 μL /min. The oil phase and water phase met at the flow-focusing junction of the microfluidic chip, where the generation of oil drops took place. The production process was monitored by high-speed camera (Optronis) at 1000 frames per second (fps) for a resolution of 800x600. The o/w emulsion was transferred from the microfluidic chip to the printing nozzle through FEP tubing (1/16" x 0.25 mm, Dolomite).

Modification of substrates. Glass cover slips (22×22 mm, thickness 0.13−0.16 mm, Academy Scientific) were loaded into a Teflon rack, soaked in 2 wt% alkaline detergent solution (Decon 90, Decon Laboratories) and sonicated for 15 minutes. Cover slips were individually rinsed with hot water and then ultra-high purity water for two minutes, dried in an oven at 100 °C for one hour and cleaned in an air plasma cleaner for half an hour. The cover slips were either used in this state as a hydrophilic substrate or they

were coated with a hydrophobic layer by vapour deposition of a silane or silazane (e.g. CDMOS or HMDS) in a vacuum desiccator for two hours. The treated coverslips were rinsed with acetone and then ultra-high purity water for two minutes and dried in an oven overnight.

Ink-jet printing. The monodisperse emulsion was transferred to a Microfab drop-on-demand device (MJ-ABP-01, Microfab Technologies; 50 or 80-μm diameter orifice) controlled by a Microfab driver unit (Microfab JetDrive III controller CT-M3-02). Emulsion drops (typical volume 150−250 pL) were generated with a bipolar waveform of ± 40−50 V and were ejected from the nozzle orifice at a velocity of ~1 m s^{-1} onto the substrate. The printed drops dried freely under ambient conditions at 21−23 °C and relative humidity of 30−35 %. For experiments at high humidity (85−90%), a humidity chamber was used. The evaporation process on the substrate was recorded from below by a high-speed camera (Photron APX RS) at 250 fps with an exposure time of 4 ms. The side profile of the drying drops was captured by a high-speed camera (Optronis) at 250 fps with an exposure time of 4 ms.

Characterization. Coverslips with dry deposits were sputtered with a conductive film of gold and imaged by scanning electron microscopy (Hitachi SU70 FEG SEM, 8 keV). Individual polymer particles were detected in the SEM images using the built-in Matlab function for the circle Hough transform, from which we calculated the size distribution and the coefficient of variation (defined as $CV = \frac{1}{d^*} \times \left[\frac{1}{n-1} \sum_{i=1}^{n} (d_i - d^*)^2 \right]^{1/2} \times 100\%$, where d_i is the measured particle diameter, d^* is the mean diameter, and n is the number of particles analysed). The contact angle of emulsion drops and the interfacial tension between the oil and water phase were measured by the sessile drop and pendant drop methods, respectively (FTÅ200, First Ten Ångstroms); each reported value was an average of three independent measurements.
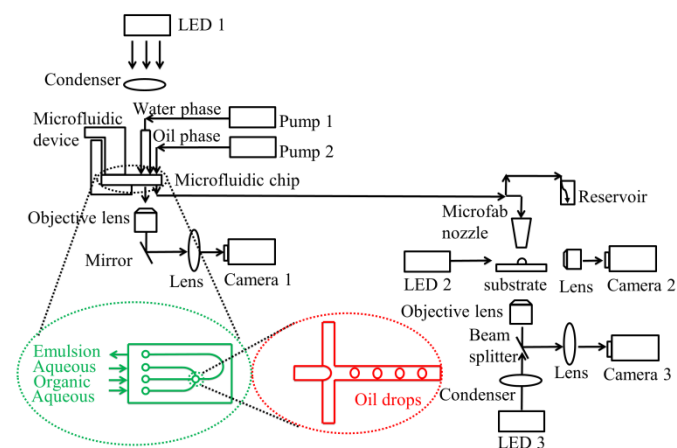

Figure 1. Schematic of experimental setup for sequential generation of an o/w emulsion by microfluidics and inkjet printing of emulsion droplets.

Results and Discussion

1. Preparation of monodisperse emulsion droplets by microfluidics

Droplet microfluidics is an efficient method for preparation of monodisperse emulsion droplets.[31-33] Figure 2a shows a set of

images recording the formation of oil drops in the flow-focussing junction: the oil flow enters through the channel at the left and the water through the channels at the top and the bottom. Droplet formation is governed by a competition between the deformation of the o/w interface achieved by viscous shear and the resistance of the interface to deformation arising from surface tension. The transition from the dripping to the jetting regime is determined by the capillary numbers of both the continuous and disperse phases,[34] and within the dripping regime, the flow rate ratio Q_o/Q_w determines the size of the drop. Stable monodisperse oil droplets were observed for varying flow rate ratios and polymer concentrations. We fixed the aqueous flow rate, Q_w, and varied the oil flow rate, Q_o. When Q_o/Q_w increased from 0.1 to 0.5, the diameter of oil droplets increased from around 6 to 12 μm (Figure 2b$_1$ and 2b$_2$). When Q_o/Q_w was > 0.5 or < 0.1, backflow of the water or oil phase took place and no oil droplets formed. The polymer concentration had only a small influence on droplet size in the range of concentrations 0.5−5 wt% because drop size depends weakly on viscosity of oil phase.[35]

The emulsions were cast onto clean substrates and allowed to dry slowly, forming a continuous monolayer of well-ordered, hexagonally packed polystyrene particles (Figure 2c), as has been observed previously in EISA of pre-formed colloidal suspensions. The particle size depends on both the oil droplet size and the PS concentration: the polystyrene particles were spherical and of uniform size with diameters of 1.04±0.02 μm, 2.2±0.05 μm, and 2.02±0.05 μm for the samples in Figures 2c$_1$, 2c$_2$ and 2c$_3$, respectively (see Figure S1 in Supplementary Information for the particle size distributions). The coefficient of variation in the particle size distribution was less than 2.5%.
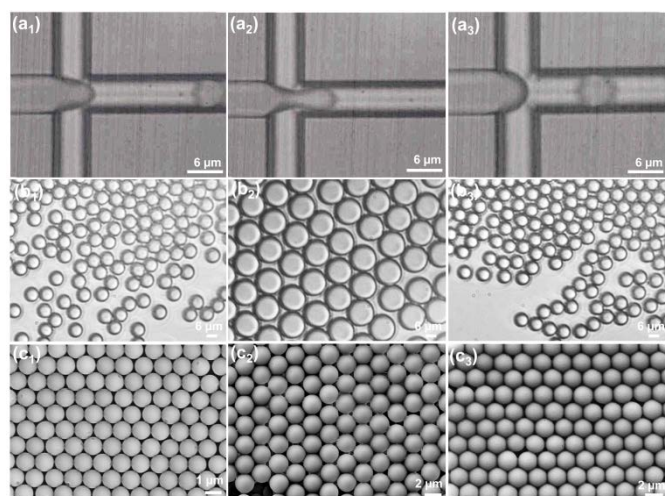

Figure 2. (a) Images showing o/w droplet production in the flow-focusing junction of the microfluidic chip; (b) Images of monodisperse emulsions produced from a continuous phase of 0.5 wt% SDS in water and a discrete phase comprising (b$_1$) 0.5 wt%, (b$_2$) 0.5 wt%, and (b$_3$) 5 wt% polystyrene in DCM. The flow rate of water phase was constant at 2 μL/min, the flow rate of oil phase was (b$_1$) 0.4 μL/min, (b$_2$) 1 μL/min, and (b$_3$) 0.4 μL/min. (c) SEM images of deposits with polystyrene particles from corresponding emulsions after free drying of a film cast on a clean glass coverslip.

2. Inkjet printing of monodisperse emulsions

Emulsion drops were printed continuously at 1 Hz through an 80-μm nozzle onto a plasma-treated glass coverslip with $\theta_{H_2O} = 20^0$. A nozzle with a large orifice was chosen to minimise the shear stress on the oil droplets. The deformation of an oil droplet in a shear flow is, to a good approximation, equal to the capillary number, $Ca = \mu_c \dot{\gamma} d / \sigma$ where μ_c is the viscosity of the continuous phase, $\dot{\gamma}$ the shear rate, d the droplet diameter and σ the interfacial tension.[36] Reducing the droplet deformation decreases the likelihood of break-up of the droplets during jetting.

Figure 3 shows images extracted from videos (see video 1 and 2 in Supplementary Information) that illustrate three distinct stages of the evaporation process. To understand what we see in these images we need to consider two factors. First, the oil is denser than water (density, ρ_{DCM} = 1.3266 g cm^{-3})[37] so the droplets sink. The sedimentation rate, v, can be roughly estimated from Stokes' law (though this neglects interactions between droplets and the proximity of the substrate): $v = \left(\rho_{DCM} - \rho_{water} \right) g d^2 / 18 \mu_c$, where g is the gravitational constant. For a 6-μm diameter droplet, $v \sim 6$ μm s^{-1}. This is sufficiently fast that sedimentation occurs in the pipework connecting the microfluidic chip to the nozzle, so the volume fraction of oil in the emulsion is not well-controlled, but is generally higher than that expected from the flow-rate ratios. The typical drying time of the DCM droplets is ~ 1 s and the typical height of a droplet at the apex is ~ 15−20 μm. Consequently, while some sedimentation does occur during drying, there is insufficient time for 6-μm droplets to settle to the bottom of the printed drop under gravity. The Peclet number is also large so Brownian diffusion does not homogenise the oil droplet distribution vertically or horizontally, though it may play a role in annealing of local defects in the deposit.

Second, although DCM is much more volatile than water (vapour pressure at 293 K, p_v = 46 kPa for DCM and 2.34 kPa for water, see Table 1), which solvent evaporates faster depends on the rate-limiting step in the mass transport of the DCM: diffusion in the aqueous phase or diffusion in the gas phase. To get a better understanding of the evaporation process we consider a simple mass transport model for DCM escaping from a layer of DCM droplets a distance δ below the air−water interface in a sessile emulsion drop of radius R and a contact angle θ. The average evaporative flux, $J_{ave,}$ in the vapour phase is given approximately by[38]

$$J_{ave} = \frac{D_{vap}}{R} c_s(\mathrm{v})(0.27\theta^2 + 1.30), \quad (1)$$

where $c_s(\mathrm{v})$ is the concentration of DCM vapour at the surface of the printed droplet, and D_{vap} = 1.08 × 10^{-5} m^2 s^{-1} is the diffusion coefficient of DCM in air[37]. For small θ, we can ignore the first term in brackets and

$$J_{ave} = \frac{1.3 D_{vap}}{R} c_s(\mathrm{v}) \quad . \quad (2)$$

Assuming that Henry's Law is valid,

$$\frac{c_s(\text{v})}{c_0(\text{v})} = \frac{c_s(\text{l})}{c_0(\text{l})}, \tag{3}$$

where $c_s(\text{l})$ is the concentration of DCM in the liquid phase at the surface and $c_0(\text{l})$ and $c_0(\text{v})$ are the saturation concentrations of DCM in the liquid (~2% by weight) and vapour phases. It is reasonable to assume that the water right next to the DCM droplets is saturated in DCM, i.e. the DCM concentration is $c_0(\text{l})$. The DCM from the emulsion droplets has to diffuse through a thickness δ of water between the emulsion droplet and the air/water interface of the drop. From Fick's first law, the flux of DCM in the liquid is

$$J = \frac{D_{liq}(c_0(\text{l}) - c_s(\text{l}))}{\delta}, \tag{4}$$

where $D_{\text{liq}} = 1.17 \times 10^{-9}\,\text{m}^2\,\text{s}^{-1}$ is the diffusion coefficient of DCM in water.[37] If we neglect the motion of the interface, the flux of DCM into the interface from the liquid side has to balance the flux of DCM out of the interface from the vapour side, so

$$\frac{D_{liq}(c_0(\text{l}) - c_s(\text{l}))}{\delta} = \frac{1.3 D_{vap}}{R} c_s(\text{v}). \tag{5}$$

Using Henry's Law, we can eliminate $c_s(\text{v})$ to obtain

$$\frac{D_{liq}(c_0(\text{l}) - c_s(\text{l}))}{\delta} = \frac{1.3 D_{vap}}{R} \frac{c_s(\text{l}) c_0(\text{v})}{c_0(\text{l})}. \tag{6}$$

Substituting, $D_{vap}/D_{liq} = 9.23 \times 10^3$ and $c_0(\text{v})/c_0(\text{l}) = 0.080$ into eq. (6) and rearranging gives

$$\frac{(c_0(\text{l}) - c_s(\text{l}))}{c_s(\text{l})} \approx 10^3 \frac{\delta}{R}. \tag{7}$$

As an example, if we take the radius of the sessile drop to be $R = 100\ \mu\text{m}$, and the contact angle to be $\theta = 20°$, the height of the drop would be 17 μm. If we then had a 6-μm droplet sitting at the bottom of the ink drop, it would be about $\delta = 10\ \mu\text{m}$ from the surface. With $\delta/R = 10$, we have $(c_0(\text{l}) - c_s(\text{l}))/c_s(\text{l}) = 10^2$, so the concentration of DCM just below the free liquid–vapour interface would be only 1% of its saturated value. Here the evaporation rate is dominated by mass transport in the aqueous phase. The consequence, however, is that the vapour pressure is only 1% of the saturated vapour pressure (~0.5 kPa) which is less than the vapour pressure of water. So the water will evaporate faster than the DCM except at very high relative humidities (RH). Near the edge of the drop, however, the thickness of the water film between the DCM droplets and the drop surface is much less – say 1 μm. Now, $(c_0(\text{l}) - c_s(\text{l}))/c_s(\text{l}) = 10$. Mass transport is still limited by diffusion through the bulk phase, but now the vapour pressure is about 10% of the saturated vapour pressure of DCM (4.6 kPa) so DCM evaporates faster than water. As the aqueous phase evaporates, the height of the droplet decreases and hence so does δ. Thus even in the centre of the drop, there will come a time when the DCM evaporates faster than the aqueous phase so the prerequisite for the emulsion solvent evaporation method to work – namely that the discrete phase evaporates before the continuous

phase – is still satisfied. For completeness, we note that near the end of the evaporation of the oil droplets, the DCM concentration in the droplets falls quickly and so does its chemical potential. This reduces $c_0(\text{l})$ and hence slows down mass transport. 'Sticky' particles containing residual DCM are undesirable since they will tend to adhere and deform rather than form mobile arrays in which defects can anneal during drying.

Turning back to Figure 3(a_1), we observe emulsion droplets throughout the droplet just after printing (also see video 1 and 2 in Supplementary Information). The droplets near the edges are in focus (i.e. near the substrate) while those in the centre are out of focus indicating that they are distributed through the volume of the drop. Even at a very early stage, the droplets near the contact line are smaller than those nearer the centre due to the fact that the evaporation rate is much faster near the contact line (J diverges as $\left(1 - (r/R)^2\right)^{-1/2}$; eq. (1) is just the average evaporation rate over the droplet.[38] In Figure 3(a_2), a layer of particles has formed near to the contact line while oil droplets are still observed near the centre, due to the height-dependence of the mass transport described above. Note that the particles are excluded from a region very near the contact line, where the height of the droplet (which is still a spherical cap) is less than the particle diameter. Particles in this region deform the liquid-vapour interface, which is energetically unfavourable. Since the particles are mobile this capillary force pushes the particles towards the apex of the drop. In Figure 3a_3, the oil droplets have all formed solid particles but the number density is such that the inward capillary force is opposed by interparticle repulsions: a uniform densely packed layer of particles is formed which defines the height of the drop. Finally, Figure 3a_4, show the particle distribution after the last of the aqueous phase has dried. In general, we observe that the size of the circular deposit is smaller than that of the initial contact line due to the inward capillary forces on the particles during drying (from 116 μm to 88 μm in diameter in this example).
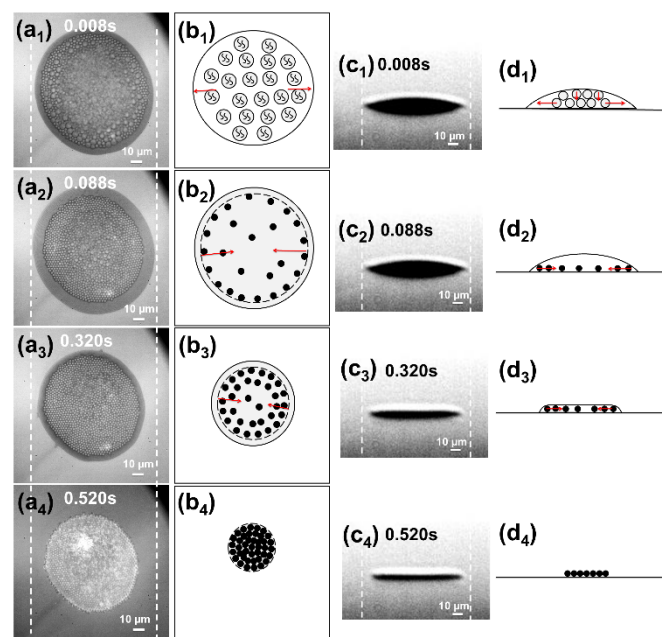

Figure 3. (a) Bottom-view optical microscopy images and (b) corresponding schematic graphs showing the evolution of a printed

emulsion droplet (66.5 mg mL^{-1} PS/DCM dispersed in 1.0 mg mL^{-1} SDS/water) with 6-µm oil drops on a plasma-treated glass cover slip. The objective is focussed near the substrate. (c) Side-view images and (d) schematic diagrams of the variations of the droplet profile. The white dashed lines in (a) and (c) indicate the maximum extent of the contact line after spreading of the emulsion droplet. The red arrows in (b) and (d) show the direction of motion of the oil drops or particles during the evaporation process.

Table 1. Properties of DCM and water at 20 °C.[37]

DCM solubility in water	$c_0(l) = 0.235$ M
Saturated DCM vapour pressure	$p_v = 46$ kPa
Water vapour pressure	$p_{v(water)} = 2.34$ kPa
Saturated DCM concentration in air	$c_0(v) = p_v/RT = 0.0189$M
DCM density	$\rho_{DCM} = 1.3266$ g cm^{-3}
0.1wt% aqueous phase viscosity	$\eta = 0.001$ Pa s

The dry deposits were analysed by scanning electron microscopy (SEM). Figure 4 shows a typical SEM image for a particle deposit from a 5 wt% PS/DCM oil phase. The range of particle diameters in this deposit is 2.212−2.686 µm, with a few much smaller particles (< 1 µm) which probably originate from satellites formed during the break-up of the primary emulsion droplets. The particles have a mean diameter of 2.48 µm and CV of 5.65%. Comparison with Figure 2 shows that the polydispersity is worse than in a cast film indicating that some coalescence or fission of emulsion droplets has occurred during printing due to the high shear stress in the nozzle or during droplet formation. Nevertheless the size distribution of the particles in the printed droplet is much narrower than in our previous study on homogenized emulsions [5], and sufficiently narrow that domains of hexagonally packed spheres are observed.
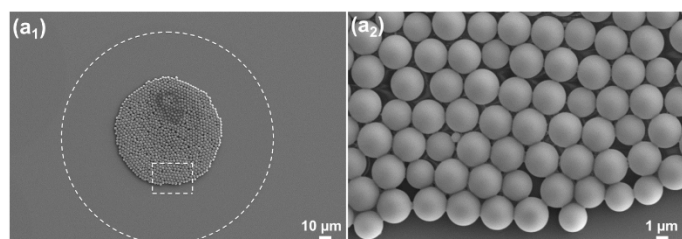

Figure 4. SEM image showing the morphology of the deposit with a monolayer of polystyrene particles from emulsions (O, 66.5 mg ml^{-1} PS/DCM; W, 1.0 mg ml^{-1} SDS/water) with 6-µm oil drops on a plasma-treated glass cover slip.

3. Effect of process parameters on polydispersity

Uniformity of particle size is an important attribute not only for the formation of ordered arrays but for any functional ink in which the morphology of the particles controls the function of the surface. For example, the wall thickness of microcapsules controls the rupture strength of the capsule and the rate of release of its contents. It is thus desirable to control the particle size within as narrow a range as possible. If the polydispersity in the particle size arises from break up of the oil droplets during printing, then the polydispersity can be improved by reducing the capillary number in one of three ways: decreasing the shear rate, decreasing the droplet size or increasing the interfacial tension between the water

and oil phase. In this study, we used an 80-µm nozzle instead of the 50-µm nozzle used in our previous work to decrease the shear rate and used the smallest DCM drops that could reproducibly be generated in the flow-focussing device (6-µm diameter). Figure 5 shows the consequences of using a smaller nozzle (50 µm; figure 5a) or larger initial oil drops (around 9 µm; figure 5b), both of which increase the deformation of the emulsion drops. In both cases the particle size distribution is broader than with the 80-µm nozzle and 6-µm DCM drops (Figure 4).
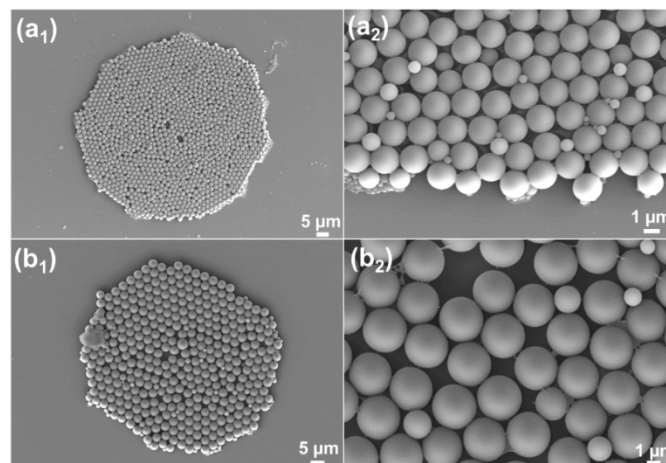

Figure 5. SEM images of drying deposits from emulsions (66.5 mg ml^{-1} PS/DCM in1.0 mg ml^{-1} SDS/water) with (a) 6-µm oil drops printed through a 50-µm nozzle, (b) 9-µm oil drops printed through an 80-µm nozzle on plasma-treated glass cover slips.

The interfacial tension depends on the concentration of the emulsifier, SDS, in the aqueous phase. Table 2 reports the DCM−water interfacial tension for various concentrations of SDS both above and below the critical micelle concentration (8.2 mM, 0.236 wt%). Above the cmc, the interfacial tension is approximately constant, while it increases rapidly as the surfactant concentration is reduced below the cmc.

Table 2. Interfacial tension between DCM containing 5 wt% polystyrene and water containing SDS.

SDS concentration (±0.01 wt%)	Interfacial tension (mN m^{-1})
0	27.5±0.5
0.05	12.4±0.5
0.1	6.5±0.3
0.2	4.9±0.1
0.3	4.7±0.1
0.5	4.5±0.1

To explore the effect of SDS concentration on the printing of emulsions, we prepared emulsions aqueous solutions with 0.05, 0.1 and 0.5 wt% of SDS. Micrographs of oil droplets inside the microfluidic chip show that emulsions were stable with SDS concentrations above 0.1 wt%, but coalescence of droplets occurred at 0.05% SDS. Figure 6 compares dry deposits of emulsions printed from 0.1 and 0.5 wt% solutions of SDS. More break up was observed in the emulsion with the lower surface tension (0.5 wt%) leading to an increased polydispersity of the particles. A surfactant concentration of 0.1 wt% provided the

optimal balance of emulsion stability and resistance to droplet deformation during printing.
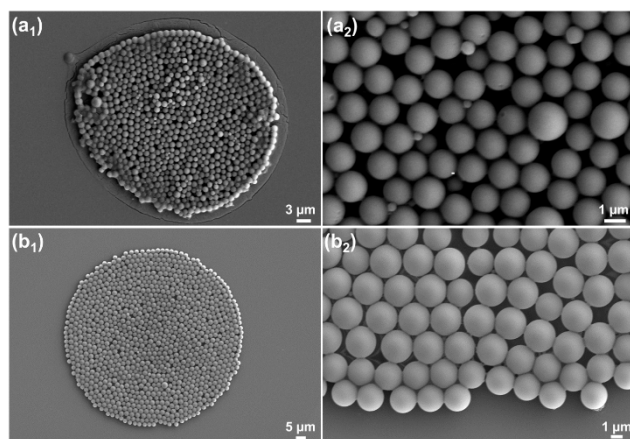

Figure 6. SEM images of drying deposits from emulsions comparing 6-µm oil drops (O, 66.5 mg ml^{-1} PS/DCM) with (a) 0.5 wt% and (b) 0.1 wt% SDS in the aqueous phase on plasma-treated glass cover slips.

The relative humidity affects the relative evaporation rates of the discrete and continuous phases. Figure 7 compares the morphology of deposits from emulsion droplets drying at an RH of (a) 85% and (b) 35%. Close-packed monolayers of particles were obtained at both humidities (a$_1$ and b$_1$), but the particles formed at high humidity were more spherical. As high humidity slows down the evaporation of aqueous phase, soft DCM drops have more time to transform into solid polystyrene particles (figure 7a$_2$) before they are compressed together under capillary forces in the latter stages of drying. In Figure 7b$_2$, showing a deposit formed at low RH, some of the particles have facetted sides suggesting that they were still soft when they interacted with their nearest neighbours. These images shows that despite the much higher volatility of DCM than water, care needs to be taken to ensure that the particles are sufficiently solvent-free before the final stages of evaporation of the continuous phase.
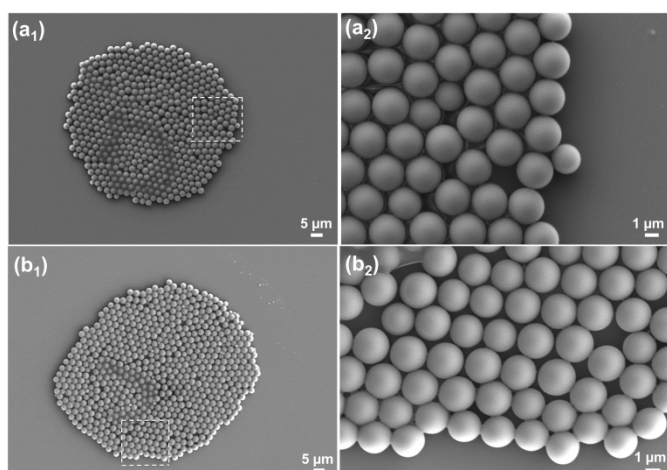

Figure 7. SEM images of deposited from emulsions (O, 66.5 mg ml^{-1} PS/DCM; W, 1.0 mg ml^{-1} SDS/water) with 6-µm oil drops dried in air at a relative humidity of (a) 85% and (b) 35% on glass cover slips treated with plasma.

4. Morphology of dry deposits

Particle size can be readily tuned through variation of the initial DCM droplet size or polymer concentration. To enable a higher monodispersity of particles and a more efficient use of DCM solvent, we use the latter method to obtain a larger particle. Emulsions containing 6-µm diameter oil droplets with two different polystyrene concentrations (0.5 wt% and 5 wt%) were printed onto plasma-treated glass coverslips. In SEM images, deposits of polystyrene particles with a mean diameter of 1.1 µm (Figure 8a) and 2.48 µm (Figure 8b) were observed. Figure 8a shows a typical pattern formed from small particles, although each deposit is different. Characteristic features are a ring-like deposit with a diameter much less than that of the initial contact line of the droplet (60 µm and 295 µm, respectively, in this example) and an irregular hole near the centre of the deposit due to pinning of the contact line in the latter stages of drying. The larger particles (Figure 8b) showed a circular deposit with a well-ordered monolayer of particles at the centre (see also Figure 4 and 6(b)). As reported above, the diameter of the deposit is smaller than the initial footprint (92 µm and 184 µm, respectively, in this drop). We rationalise the different behaviour in terms of the capillary force acting on the particles when they deform the interface near the contact line.[39] For the larger particles, the capillary force is sufficient to overcome the friction between the particles and the substrate until a closely-packed deposit is formed. For the smaller particles, the capillary force is weaker and the contact line pins before a continuous layer of particles is formed, leading to a ring-like deposit. The hole in the centre arises from outward capillary flows consequent on evaporation with a pinned contact line (the coffee-ring effect). In our previous study[5], with a polydisperse mixture of particles we observed that on a hydrophilic substrate ($\theta_{H_2O} = 20^o$) there was size segregation with larger particles concentrated in the central deposit with some small particles deposited at larger radial distances, consistent with the idea that the capillary forces on small particles are less able to overcome the friction with the substrate.
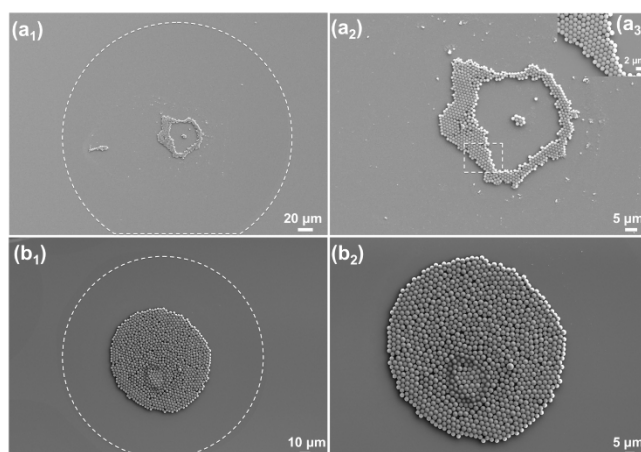

Figure 8. SEM images of deposits from emulsions comprising (a) 6.7 mg ml^{-1} and (b) 66.5 mg ml^{-1} PS/DCM in 1.0 mg ml^{-1} SDS/water with 6-µm oil drops on plasma-treated glass cover slips.

Why small (non-Brownian) particles should be less mobile than large particles can be rationalised in simple physical terms. The increase in surface area of the air−water interface due to

deformation by a rigid particle scales with the surface area of the particle i.e as R^2, where R is the particle radius. If the interaction between the particle and the solid surface arises primarily from dispersion interactions (both particle and surface are negatively charged, so the short-range double-layer forces are repulsive), then the interaction energy between the particle and the surface scales linearly with R.[40] From Hertzian mechanics, the radius, a, of the contact between a spherical particle and planar surface scale as $(LR)^{1/3}$, where L is the load.[41] Thus the contact area scales as $R^{4/3}$. If the friction with the surface depends on the contact area, then the friction decreases more slowly with R than does the capillary force; hence smaller particles are more likely to pin the contact line. Furthermore, the pressure scales as $R^{-1/3}$, so from DLVO theory the thickness of the aqueous film increases with increasing R, which will also reduce the friction due to viscous drag in the thin film between the particle and the substrate.[40] An alternative explanation is that the smaller particles cover a smaller surface area and thus would form a dense deposit later in the drying cycle, when the concentration of the dispersant is much higher. If the dispersant (in this case, SDS) were to form a viscous solution or mesophase at high concentrations (which are only achieved in the last stages of drying), then this increase in viscosity might also hinder the mobility of particles near the contact line.

Formation of sub-micron particles is possible by reducing the polymer concentration in the DCM, but the number of particles is limited by the number of DCM droplets, so a rather sparse deposit is likely to occur unless the number of droplets is increased. This entails reducing the size of the emulsion droplets, which is challenging in microfluidics. Production of particles larger than ~ 3 μm requires larger emulsion droplets and/or higher polymer concentrations. The upper limit on particle size is limited by break-up of large droplets during printing and by the viscosity range that yields droplet formation in the flow-focussing junction. The emulsion solvent evaporation method in inkjet printing is thus best for micron-sized particles rather than nanoparticles or larger particles.

Compared to the cast-drying emulsion, the inkjet-printed emulsion drop and EISA of colloidal suspension form deposits with a lower degree of crystalline order, due to the grain boundaries with defects or cracks in the circular deposits. During drying, the inward capillary force pushed particles to the droplet centre from all directions, hindering the formation of close-packed hexagonal arrays.

Influence of the underlying glass slip

Previous studies have demonstrated that the wetting properties of the substrate influence the deposit pattern.[5, 6, 13, 28, 42] Figure 8 compares deposits formed from emulsions with 0.5 wt% and 5 wt% polystyrene in the oil phase on substrates with two different wettabilities: plasma-treated glass coverslips ($\theta_{H_2O} = 20°$) and HDMS-treated coverslips ($\theta_{H_2O} = 64°$). The 1.1-μm particles formed a ring-like deposit on the hydrophilic substrate and a close-packed monolayer on the more hydrophobic substrate. The 2.48-μm particles formed a close-packed monolayer on the hydrophilic substrate and a multilayer on the more hydrophobic substrate. The maximum diameter of the contact line on the hydrophilic substrate (Figure 9 a_1 and b_1) is ~2 times that on the hydrophobic substrate (Figure 9 a_2 and b_2) due to the stronger wetting of the hydrophilic

surface. Higher contact angles lead to large capillary forces, since the variation in the deformation energy of the surface with the radial position of a particle depends on the slope of the air–liquid interface. For the smaller particles, the increased capillary force is sufficient to prevent pinning. For the larger particles, it can displace particles from the monolayer to form multilayer structures. In addition, the smaller contact radius reduces the distance that the small particles are dragged by the contact line, reducing the opportunities for pinning. For the larger particles, the greater height of the droplet increases the sedimentation time and it is likely that particles from DCM droplets initially near the upper surface of the droplet deposit on top of layers of particles underneath. This study shows the importance of controlling the wettability to obtain uniform, ordered monolayers of particles. It is possible that a monolayer of the larger particles could also be formed on the hydrophobic substrate if the volume fraction of oil (and hence the number of particles) was reduced, but this parameter is not well-controlled in our experiment owing to sedimentation in the tube connecting the microfluidic device to the inkjet nozzle. Close-coupling of the microfluidic chip and the inkjet nozzle would eliminate this issue.
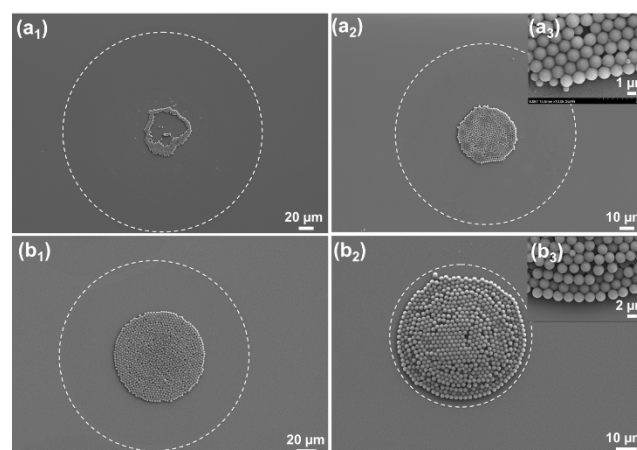

Figure 9. SEM images of deposits of (a) 1.1 μm and (b) 2.48 μm particles on (a_1, b_1) hydrophilic and (a_2, b_2) hydrophobic glass coverslips. The insets (a_3, b_3) show enlarged images of the edge of the deposits. The dashed line shows the maximum contact diameter of the emulsion drop.

Conclusion

We have demonstrated a strategy to obtain uniform monolayers of polymeric particles by inkjet printing of monodisperse oil-in-water emulsions generated by microfluidics. There is a small increase in the polydispersity of the particles compared to the emulsion (CoV in the particle diameter <6% under optimised conditions) which is ascribed to break-up and coalescence of oil droplets during jetting. The polydispersity is minimised by minimising the capillary number during jetting through three strategies: increasing the nozzle diameter to reduce the shear rate, increasing the oil–water interfacial tension and reducing the oil droplet size. The particle size is controlled by the polymer concentration in the oil phase. Relative humidity plays a minor role in the particle formation process. At low RH, the water droplet evaporates faster and some faceting of the particles was observed due to residual solvent in the

PS particles as they pack into the monolayer. The effect of the substrate wettability on the morphology of the deposit was briefly explored: well-ordered monolayers of small particles formed on hydrophobic substrates and of large particles on hydrophilic substrates.

The objective of this work has been to explore the effect of process parameters on the combined microfluidic/inkjet method for generating uniform layers of particles. For this reason we only used a single chemical system: polystyrene in DCM as the oil phase and SDS solutions as the aqueous phase. The emulsion solvent evaporation method does, however, have wide applicability in terms of polymers, organic solvent[5] and morphology of the particles formed. It can also be used to incorporate functional cargoes. In a subsequent paper, we will explore the encapsulation of functional cargoes in the polymeric particles formed during the drying of inkjet-printed emulsions. Major benefits of combining the generation of the emulsion and inkjet printing are the reduction of nozzle clogging and avoidance of shelf-life issues since there is no need to stabilise a particle suspension against aggregation and sedimentation.

Conflicts of interest

There are no conflicts to declare.

Supporting Information.

Supporting information includes histograms of particle sizes. The following file is available free of charge via the Internet at http://pubs.acs.org.

Acknowledgements

References

The authors declare no competing financial interest.

1.   A. Utada, E. Lorenceau, D. Link, P. Kaplan, H. Stone and D. Weitz, *Science*, 2005, **308**, 537-541.

2.   S. Liu, R. Deng, W. Li and J. Zhu, *Adv. Funct. Mater.*, 2012, **22**, 1692-1697.

3.   Y. Zhao, Y. Cheng, L. Shang, J. Wang, Z. Xie and Z. Gu, *Small*, 2015, **11**, 151-174.

4.   J. Wang, Y. Hu, R. Deng, W. Xu, S. Liu, R. Liang, Z. Nie and J. Zhu, *Lab Chip*, 2012, **12**, 2795-2798.

5.   R. Deng, L. Yang and C. D. Bain, *ACS Appl. Mater. Interfaces*, 2018, **10**, 12317-12322.

6.   J. Sun, B. Bao, M. He, H. Zhou and Y. Song, *ACS Appl. Mater. Interfaces*, 2015, **7**, 28086-28099.

7.   J. Wang, L. Wang, Y. Song and L. Jiang, *J. Mater. Chem. C*, 2013, **1**, 6048-6058.

8.   J. Hou, M. Li and Y. Song, *Angew. Chem.*, 2018, **57**, 2544-2553.

9.   M. Kuang, L. Wang and Y. Song, *Adv. Mater.*, 2014, **26**, 6950-6958.

10. M. Singh, H. M. Haverinen, P. Dhagat and G. E. Jabbour, *Adv. Mater.*, 2010, **22**, 673-685.

11. H. P. Le, *J. Imaging Sci. Technol.*, 1998, **42**, 49-62.

12. J.-U. Park, M. Hardy, S. J. Kang, K. Barton, K. Adair, D. kishore Mukhopadhyay, C. Y. Lee, M. S. Strano, A. G. Alleyne and J. G. Georgiadis, *Nat. Mater.*, 2007, **6**, 782.

13. J. Park, J. Moon, H. Shin, D. Wang and M. Park, *J. Colloid Interface Sci.*, 2006, **298**, 713-719.

14. E. Sowade, T. Blaudeck and R. R. Baumann, *Cryst. Growth Des.*, 2016, **16**, 1017-1026.

15. H. Ding, C. Zhu, L. Tian, C. Liu, G. Fu, L. Shang and Z. Gu, *ACS Appl. Mater. Interfaces*, 2017, **9**, 11933-11941.

16. K. N. Al-Milaji, R. R. Secondo, T. N. Ng, N. Kinsey and H. Zhao, *Adv. Mater. Interfaces*, 2018, **5**, 1701561.

17. J. Hou, H. Zhang, Q. Yang, M. Li, Y. Song and L. Jiang, *Angew. Chem.*, 2014, **53**, 5791-5795.

18. B. M. Boyle, T. A. French, R. M. Pearson, B. G. McCarthy and G. M. Miyake, *ACS Nano*, 2017, **11**, 3052-3058.

19. Y. Xia, B. Gates, Y. Yin and Y. Lu, *Adv. Mater.*, 2000, **12**, 693-713.

20. R. Bhardwaj, X. Fang, P. Somasundaran and D. Attinger, *Langmuir*, 2010, **26**, 7833-7842.

21. M. Anyfantakis, Z. Geng, M. Morel, S. Rudiuk and D. Baigl, *Langmuir*, 2015, **31**, 4113-4120.

22. Y. Guo, L. Li, F. Li, H. Zhou and Y. Song, *Lab Chip*, 2015, **15**, 1759-1764.

23. N. D. Patil, R. Bhardwaj and A. Sharma, *Langmuir*, 2018.

24. Y. Yin, Y. Lu, B. Gates and Y. Xia, *J. Am. Chem. Soc.*, 2001, **123**, 8718-8729.

25. T. Still, P. J. Yunker and A. G. Yodh, *Langmuir*, 2012, **28**, 4984-4988.

26. J. Wang, Y. Hu, R. Deng, R. Liang, W. Li, S. Liu and J. Zhu, *Langmuir*, 2013, **29**, 8825-8834.

27. J. Park and J. Moon, *Langmuir*, 2006, **22**, 3506-3513.

28. L. Cui, Y. Li, J. Wang, E. Tian, X. Zhang, Y. Zhang, Y. Song and L. Jiang, *J. Mater. Chem.*, 2009, **19**, 5499-5502.

29. L. Bai, Z. Xie, W. Wang, C. Yuan, Y. Zhao, Z. Mu, Q. Zhong and Z. Gu, *ACS Nano*, 2014, **8**, 11094-11100.

30. M. Liu, J. Wang, M. He, L. Wang, F. Li, L. Jiang and Y. Song, *ACS Appl. Mater. Interfaces*, 2014, **6**, 13344-13348.

31. G. M. Whitesides, *Nature*, 2006, **442**, 368.

32. Z. Nie, F. Deiss, X. Liu, O. Akbulut and G. M. Whitesides, *Lab Chip*, 2010, **10**, 3163-3169.

33. M. T. Guo, A. Rotem, J. A. Heyman and D. A. Weitz, *Lab Chip*, 2012, **12**, 2146-2155.

34. J. Nunes, S. Tsai, J. Wan and H. Stone, *J. Phys. D: Appl. Phys.*, 2013, **46**, 114002.

35. D. Zhang and H. Stone, *Phys. Fluids*, 1997, **9**, 2234-2242.

36. G. I. Taylor, *Proceedings of the Royal Society of London. Series A, Containing Papers of a Mathematical and Physical Character*, 1934, **146**, 501-523.

37. D. R. Lide, *CRC handbook of chemistry and physics*, CRC press, 2004.

38. R. G. Larson, *AIChE J.*, 2014, **60**, 1538-1571.

39. B. M. Weon and J. H. Je, *Phys. Rev. E*, 2010, **82**, 015305.

40. J. N. Israelachvili, *Intermolecular and surface forces*, Academic press, 2011.

41. K. L. Johnson and K. L. Johnson, *Contact mechanics*, Cambridge university press, 1987.

42. M. Kuang, J. Wang, B. Bao, F. Li, L. Wang, L. Jiang and Y. Song, *Adv. Opt. Mater.*, 2014, **2**, 34-38.